Remote Sensing Letters

ISSN: 2150-704X (Print) 2150-7058 (Online) Journal homepage: http://www.tandfonline.com/loi/trsl20

Radiometric calibration of a dual-wavelength terrestrial laser scanner using neural networks

Lucy A. Schofield, F. Mark Danson, Neil S. Entwistle, Rachel Gaulton & Steven Hancock

To cite this article: Lucy A. Schofield, F. Mark Danson, Neil S. Entwistle, Rachel Gaulton & Steven Hancock (2016) Radiometric calibration of a dual-wavelength terrestrial laser scanner using neural networks, Remote Sensing Letters, 7:4, 299-308, DOI: 10.1080/2150704X.2015.1134843

To link to this article: http://dx.doi.org/10.1080/2150704X.2015.1134843

Published online: 14 Jan 2016.

REMOTE SENSING LETTERS, 2016
VOL. 7, NO. 4, 299–308
http://dx.doi.org/10.1080/2150704X.2015.1134843

Taylor & Francis
Taylor & Francis Group

Radiometric calibration of a dual-wavelength terrestrial laser scanner using neural networks

Lucy A. Schofield[a], F. Mark Danson[a], Neil S. Entwistle[a], Rachel Gaulton[b] and Steven Hancock[c]

[a]School of Environment and Life Sciences, University of Salford, Salford, UK; [b]School of Civil Engineering & Geosciences, Newcastle University, Newcastle upon Tyne, UK; [c]Environment and Sustainability Institute, University of Exeter, Penryn, UK

ABSTRACT

The Salford Advanced Laser Canopy Analyser (SALCA) is a unique dual-wavelength full-waveform terrestrial laser scanner (TLS) designed to measure forest canopies. This article has two principle objectives, first to present the detailed analysis of the radiometric properties of the SALCA instrument, and second, to propose a novel method to calibrate the recorded intensity to apparent reflectance using a neural network approach. The results demonstrate the complexity of the radiometric response to range, reflectance, and laser temperature and show that neural networks can accurately estimate apparent reflectance for both wavelengths (a root mean square error (RMSE) of 0.072 and 0.069 for the 1063 and 1545 nm wavelengths, respectively). The trained network can then be used to calibrate full hemispherical scans in a forest environment, providing new opportunities for quantitative data analysis.

ARTICLE HISTORY
Received 19 August 2015
Accepted 12 December 2015

1. Introduction

Terrestrial laser scanners (TLS) measure range with very high accuracy, driving a dramatic shift in three-dimensional (3D) visualization and analysis for both natural and manmade scenes. Along with the acquisition of range from multiple azimuth and zenith angles, laser scanning systems also measure intensity, which can be related to laser power, for each laser pulse. Intensity is recorded as a sensor-specific digital number (DN) and is affected by several factors as defined in the lidar equation (Wagner et al. 2006):

$$P_r = \frac{P_t D_r^2}{4\pi R^4 \beta_t^2}\sigma, \tag{1}$$

where P_r is the received energy, P_t the outgoing laser pulse energy, D_r the aperture diameter of the receiver optics, R the distance from the laser to the target, β_t^2 the beam divergence, and σ is the backscatter cross-section, computed as:

CONTACT Lucy A. Schofield l.a.schofield@edu.salford.ac.uk School of Environment and Life Sciences, University of Salford, Salford, UK

$$\sigma = \frac{4\pi}{\Omega}\rho A_s, \tag{2}$$

where Ω is the phase function, ρ the reflectivity of the scatterer, and A_s is the illuminated area of the scattering element. Intensity information has been most commonly used to support the visual examination of point clouds but among the latest advances in laser scanning is the application of intensity data to extract information about target properties, through the interpretation of physical backscattering characteristics (Höfle and Pfeifer 2007). As a result, the reliability of the intensity measure and the application of correction methods to facilitate its effective interpretation are becoming important areas of study (Kaasalainen et al. 2009).

In order to convert raw DN recorded by the instrument into physical units related to target reflectance, it is necessary to apply a radiometric calibration procedure. In remote sensing, this is typically implemented by applying a sequence of corrections to translate the DN into a value proportional or equal to target reflectance, usually with the aid of known external reference targets (Wagner et al. 2008; Kaasalainen et al. 2009). The calibrated output, the *apparent reflectance*, is related to physical characteristics of the target and can therefore be used in object classification, change detection, and in point cloud processing algorithms for both airborne laser scanner (ALS) and TLS datasets.

Very few published studies exist on TLS radiometric calibration methods. One reason is that the design of commercial laser scanners is often undisclosed by the manufacturers and some systems have proprietary calibration routines that are performed within the system software. As a consequence, uncertainties remain which hinder the interpretation of data from many systems and limit the utilization of recorded intensity.

The Salford Advanced Laser Canopy Analyser (SALCA) is an experimental TLS instrument developed by the University of Salford and Halo Photonics Ltd. Full access to the instrument design and raw data provides an opportunity to investigate the intensity response and develop a robust radiometric calibration routine. SALCA is a dual-wavelength full-waveform TLS system: two independent lasers at wavelengths 1063 and 1545 nm are used and the entire backscattered signal for each laser pulse is recorded. The purpose is to aid the spectral separation of leaf and woody material in forest ecosystems, a current limitation of single wavelength TLS instruments. A description of the instrument including background on the development and full technical specifications may be found in Danson et al. (2014). Accurate radiometric calibration of SALCA data is a fundamental first step for inferring characteristics of the forest ecosystem such as achieving leaf and wood separation based on reflectance, along with other ecological applications, such as measuring moisture content or monitoring tree health in a forest (Gaulton et al. 2013). The main objectives and contributions of this article are:

- to assess the radiometric characteristics of the SALCA instrument; specifically, the intensity response to range, reflectance, and laser temperature,
- to develop, test, and assess the novel application of neural networks to provide a rapid and robust method for intensity correction to apparent reflectance.

2. Background to calibration

Assuming the sensor configuration for a given TLS instrument remains constant, the return power of a laser pulse is governed by the range, reflectance properties of the

target, incidence angle, and amount of beam occupied. Atmospheric effects can also play a part but are only significant over long ranges (Wagner et al. 2006).

The theoretical range dependence of laser return power can be expressed as $1/R^2$ where R is the range of the target measured, deduced from (1). Although this has been shown to be mostly valid for ALS (Höfle and Pfeifer 2007), the inverse square law does not fully apply for many TLS systems. Typically, close to the scanner, the recorded intensity increases with range: a strong deviation from the inverse square law of the lidar equation and an artefact identified for several TLS instruments (Ramirez, Armitage, and Danson 2013). This can be the result of system software such as a brightness reducer in the detector for short distances, as is the case for Faro and Leica instruments (Kaasalainen, Jaakkola, et al. 2011), or the incomplete overlap of the laser beam and detector field of view (FOV) which restricts the amount of energy reaching the detector through the optics (Höfle 2014). For longer range measurements, intensity begins to decrease as the $1/R^2$ effect becomes dominant.

The reflectance properties of the target are a significant factor controlling the amount of backscatter returned to the sensor, together with the phase function which describes reflectance as a function of angle of incidence. Assuming that the target fills the entire footprint of the laser beam and incidence angle remains constant, then the recorded intensity should increase as the reflectance of the object increases (Wagner et al. 2006).

A third factor to consider is the influence of laser temperature. It is well documented in manufacturer guidelines that many commercial TLS sensors will only function properly when used within a certain range of external temperatures. Temperatures inside the scanners may be considerably higher than the surrounding atmosphere due to laser operation and external heating, and this heating of the lasers can influence outgoing (P_t) laser pulse energy. Previous deployment of the SALCA instrument exposed a drop in received power over time from the beginning of a scan; and this has been attributed to an internal thermal effect. In an effort to cool the system, fans were installed within the scanner but a decrease in recorded intensity over time is still observed. The influence of internal temperature of the sensor on intensity has not been openly reported for other TLS systems. However, the dependence of laser power on temperature is well known (Welford and Mooradian 1982) and therefore commercial laser scanning companies must account for this effect within their algorithms, although these corrections remain inaccessible due to commercial sensitivity.

2.1. *Calibration approaches*

There are two broad approaches that can be adopted to perform radiometric calibration of TLS data. The first involves applying a series of corrections based on theoretical laws and relationships in the lidar Equation (1). These known characteristics of a laser give the received power as a function of sensor parameters, measurement geometry, and the scattering properties of the target. Wagner et al. (2008) demonstrated this approach on full-waveform ALS data collected with the RIEGL LMS-Q560 instrument (RIEGL, Horn, Austria). However, the complex non-linear interaction of TLS optics and electronics make it difficult to derive an entirely theoretical approach. This has meant that a second approach to calibration, a data-driven method, has often been preferred (Pfeifer et al. 2008). Data-driven approaches fit statistical models to empirically measured data using simple or complex non-linear fitting. For

instance, Balduzzi et al. (2011) corrected TLS intensity from a Faro LS880 with regard to distance and angle of incidence with leaf surfaces. In addition, Kaasalainen et al. (2008) describe a calibration procedure using reference targets in both laboratory and field conditions for the hyperspectral lidar prototype (HSL; Hakala et al. 2012) compared with results from ALS. Semi-empirical approaches have also been adopted, combining empirical methods to physical principles of lidar systems (Kaasalainen, Pyysalo, et al. 2011). A calibration model has been developed for the Dual-Wavelength Echidna Lidar (DWEL; Douglas et al. 2015) which combines a function to remove the effects of telescope efficiency with the inverse square law (Li et al. 2015).

The radiometric properties of the SALCA instrument are characterized by non-linearity in reflectance and temperature response, and a near-field peak followed by the inverse square form with range. Although possible, correcting for these artefacts along with saturation and near-noise signal with a function fitting approach would not be a trivial task. In contrast, neural networks offer an empirical data-driven framework which allows for non-linear relationships between inputs and outputs developed by supervised learning. Neural networks provide a powerful and flexible computational tool which can solve complex problems whilst being relatively quick and easy to implement and therefore potentially offer an alternative method to rapidly correct recorded intensity to apparent reflectance.

2.2. *Neural Networks*

Neural networks are adaptive statistical models inspired by the way in which biological nervous systems, such as the brain, process information (Abdi, Valentin, and Edelman 1999). The network structure is typically arranged in layers (input layer, hidden layer(s), output layer) with interconnected 'nodes'. Supervised learning is used to train the network until a particular input leads to a specific target output by adjusting the connection weights using an iterative error back-propagation algorithm (Abdi, Valentin, and Edelman 1999). This functionality allows application to complex systems that are not easily modelled with a closed-form equation such as the radiometric properties of some TLS sensors.

3. Methods

To establish the relationships between intensity, range, and reflectance, an external reference target of known reflectance was used. The target consisted of six subpanel squares (25 cm · 25 cm) painted onto a medium-density fibreboard (MDF) base using a mixture of white and black matte paint. The reflectivity of each subpanel was measured ten times with an ASD spectroradiometer using a contract probe to obtain the mean measured reflectance shown in Table 1. Subpanel 5 was re-painted during data collection to a reflectance of 44.13% and 40.38% for the 1063 and 1545 nm wavelengths, respectively, in order to ensure that this reflectivity region was sufficiently represented. The panel was mounted on a tripod and imaged at different ranges, during the acquisition of full hemisphere scans in a forest environment for related work. This was achieved by moving the panel around the scanner as the scan progressed, so that it was imaged multiple times at multiple ranges during each scan. At 10 m the beam footprints are approximately 0.80 cm in the 1063 nm wavelength and 0.92 cm in the 1545 nm wavelength. The panel was erected at approximately the same height relative to the scanner and visually aligned perpendicular to the laser output to reduce incidence angle effects.

Table 1. Reflectance (%) measured with an ASD spectroradiometer using a contact probe for each of the six 25 cm · 25 cm sub-panels. Mean values from 10 measurements at the two wavelengths of the SALCA instrument. Standard deviation shown in brackets.

Subpanel	Reflectance at 1063 nm (%)	Reflectance at 1545 nm (%)
1	88.78 (0.45)	80.36 (0.21)
2	27.61 (0.57)	24.50 (0.40)
3	17.08 (0.32)	15.24 (0.38)
4	9.99 (0.97)	8.77 (1.02)
5	6.15 (0.45), 44.13 (0.63)	5.55 (0.54), 40.38 (1.05)
6	3.46 (0.04)	3.53 (0.05)

High resolution (0.06° in both azimuth and zenith), full hemispherical scans were acquired between April 2014 and November 2014 in Delamere Forest, Cheshire, UK, a mixed broadleaf coniferous forest, owned and managed by the Forestry Commission, UK (Ramirez, Armitage, and Danson 2013). As a proxy for laser temperature, thermocouples were attached to the casings of the two laser units inside the instrument. These readings were logged at ten minute intervals throughout the two hour scans. Typically, two or three scans would be acquired over the course of a field day.

The raw binary files recorded by the sensor were processed to extract intensity and range for each return using the Centre of Gravity method which sums the waveform value above a predetermined threshold (Hancock et al. 2015). The mean intensity value of each sub-panel was extracted by averaging footprints over selected surface areas for both wavelengths. Each mean intensity and range value extracted from the point clouds was then attributed a laser temperature value linearly interpolated from the recorded logs.

The creation, training, and simulation of neural networks in this study were carried out using Matlab® with the Neural Network Toolbox®. The first stage was to assemble the data from the field target panels. The resultant dataset contained 868 sub-panel measurements taken from 46 scans covering ranges 1.9–32.9 m, and laser case temperatures 21.9–36.6°C and 20.2–36.9°C for the 1063 and 1545 nm lasers, respectively.

The dataset was randomly divided into three subsets: training (70%), to initiate the gradients and adjust the network weights; validation (15%), to minimize over-fitting; testing (15%), to test the final network solution. A feed-forward network object was created and an experimental approach adopted to define the optimal architecture which is shown in Figure 1. Through supervised learning, these network properties allow for non-linear relationships, an increase in training accuracy using error back-propagation, and achieve a balance between the power of the network to learn complex relationships and over-fitting.

The networks were retrained twenty times and the networks chosen with the lowest error (RMSE). Finally, the neural network was simulated with full field scans to provide an apparent reflectance output for the entire forest point cloud.

4. Results and discussion

4.1. *Radiometric characteristics*

A negative relationship was observed between the recorded laser temperature and the intensity response of all six subpanels. Figure 2 shows the results of 190 sub-panel measurements at 10 m range. A steeper slope for the 1545 nm wavelength was evident with a stronger correlation (coefficient of determination (R^2) values between 0.78 and 0.92; second order polynomial) compared with the 1063 nm wavelength (R^2 values between 0.65 and 0.82; linear fitting).

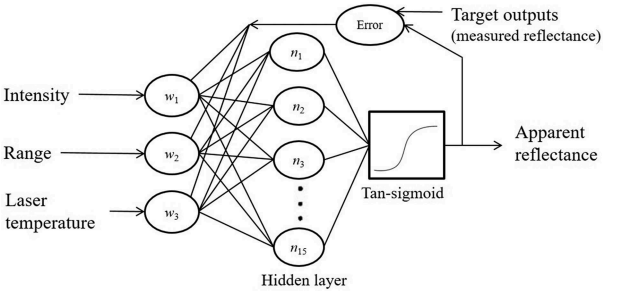

Figure 1. Feed-forward neural network architecture.

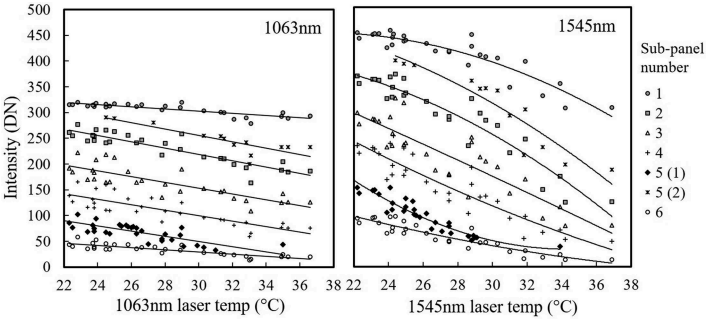

Figure 2. Relationship between laser case temperature and intensity for the six sub-panels at a range of 10 m for wavelength 1063 nm (left) and 1545 nm (right). Each sub-panel is represented by a different symbol. The 1063 nm wavelength displays a linear trend whereas the 1545 nm wavelength was best described with non-linear fitting (2nd order polynomial).

Intensity as a function of range is displayed in Figure 3 for both wavelengths showing the results of 122 measurements of subpanel 3. At close ranges, the flattened top is caused by the incomplete overlap of the laser beam and the detector field of view and then the inverse square effect becomes dominant from around 8 m. The vertical spread of data at each range can be attributed to the thermal effects described above, which also explains the larger variation in the 1545 nm wavelength.

A positive non-linear relationship between intensity and reflectance was observed. Figure 4 shows recorded intensity as a function of measured reflectance for one multi-reference panel measurement at two different laser case temperatures. As the laser case temperature

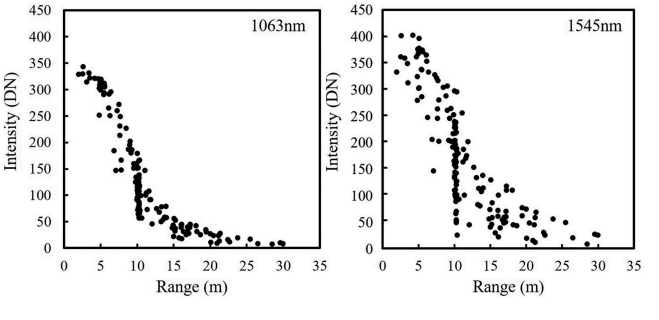

Figure 3. SALCA intensity response to range for both wavelengths: 1063 nm (left) and 1545 nm (right) for subpanel 3.

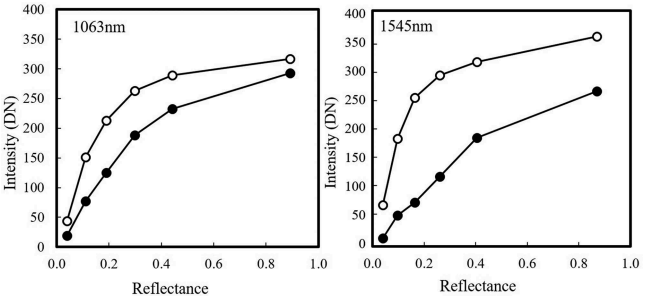

Figure 4. SALCA intensity reflectance response for both wavelengths: 1063 nm (left) and 1545 nm (right) at a range of 10 m for the six subpanels at two laser case temperature measures: 21°C (open circles) and 31°C (closed circles).

increased, the recorded intensity for a given reflectance decreased. Once again, larger intensity variation between the laser case temperatures was seen for the 1545 nm wavelength.

The results outlined above show that a temperature dependent decrease in P_t is present, which is non-linear for 1545 nm wavelength and linear for 1063 nm. This, coupled with the non-linear and non-monotonic variation in recorded intensity with range, and an observed non-linear response of the detector in both wavelengths, makes empirical function fitting difficult. The following section investigates a neural network approach to perform the calibration to test whether this approach may be used for the SALCA instrument.

4.2. *Apparent reflectance*

The selected neural networks which showed the most accurate results had an average error of 7.2% reflectance for the 1063 nm wavelength and 6.9% reflectance for the 1545 nm wavelength (Figure 5). These results are comparable with calibration fitting of the DWEL instrument of 8.1% (1064 nm laser) and 6.4% (1548 nm laser) (Li et al. 2015). Independent measurements of the directional reflectance properties of the panels were acquired in the laboratory using the ASD fibre optic cable fitted with an 8° field of view lens, at multiple view angles. These results indicated that variations in laser incidence angle for very short range measurements may result in a maximum of 5% reflectance difference, accounting for some of the scatter in Figure 5. At longer ranges the range of incidence angles is much smaller and so the effects become negligible.

A neural network output for a subset of a full point cloud is illustrated in Figure 6 for both wavelengths, along with the apparent reflectance frequency distribution of the full scan. The dataset was acquired on the 19 June 2014 under full leaf conditions for a broadleaf deciduous plot at Delamere Forest, UK, composed of Common beech (*Fagus sylvatica*) trees.

A very small number (0.14% in 1063 nm wavelength and 1.62% in 1545 nm wavelength) of the estimated apparent reflectance values were outside of the range 0–1 reflectance. Neural networks do not have the ability to accurately extrapolate beyond the range of inputs for which they have been trained (Abdi, Valentin, and Edelman 1999), therefore this hinders the performance of the network if the training dataset does not span the full intensity, range, and temperature variation of the full field scans. An examination of these anomalies revealed that their inputs were outside (or near the limits) of the training dataset. To solve this issue and increase the networks accuracy to new data, more data should be included in the training stage of the neural network development, particularly around the limits of the current dataset.

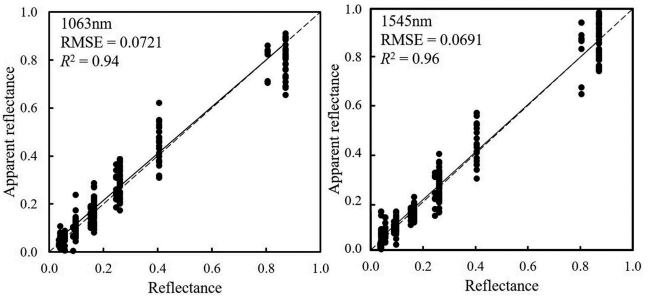

Figure 5. Relationship between apparent reflectance and measured reflectance for the test dataset: A random sample of 169 sub-panels was used to test the performance of the network. Dashed line is 1:1 fit. Solid line is least square regression line.

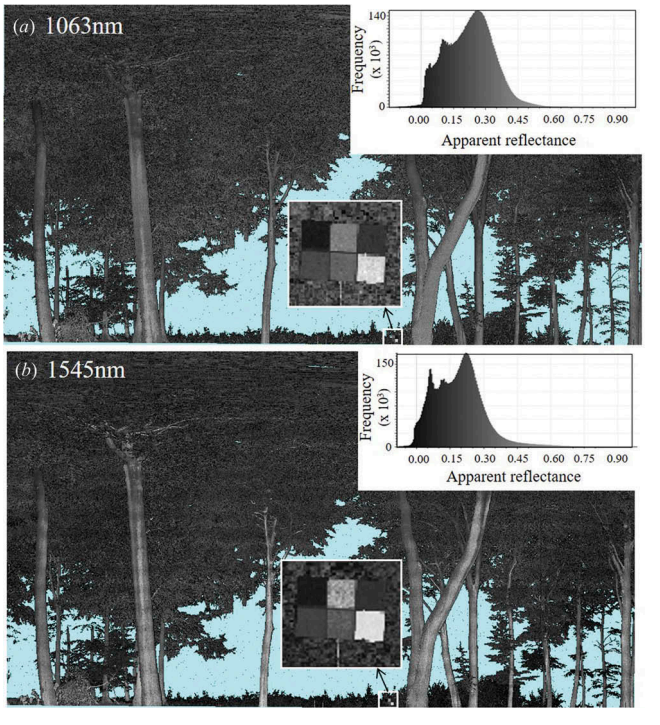

Figure 6. Subset from a full calibrated forest point cloud for (a) 1063 nm and (b) 1545 nm wavelength showing all returns. Dataset acquired on 19 June 2014 at Delamere Forest, UK. Blue background colour symbolizes no returns. Insets: histograms of apparent reflectance values for full scan (frequency in thousands) and enlarged reflectance panel at a range of 16.6 m.

Furthermore, the calibration will be most accurate at 10 m as this is where the largest proportion of the reference panels was located.

In order to assess the reliability of the network, two calibrated forest scans acquired on consecutive days in leaf-off conditions, are compared. Figure 7 shows that the neural network produces a stable output in both wavelengths.

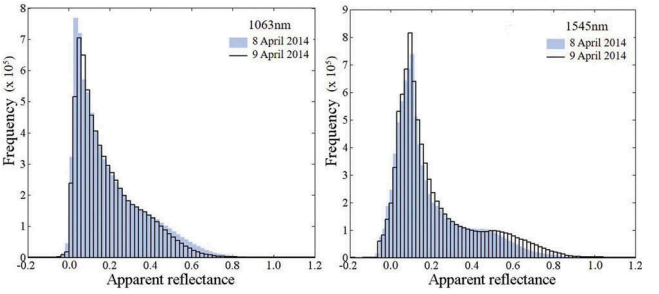

Figure 7. Frequency distribution of apparent reflectance from two scans acquired on consecutive days in leaf-off conditions (8 and 9 April 2014).

5. Conclusion

The ability to generate apparent reflectance from a laser scanning system is essential for inferring information on target properties. In forest environments, this relates to data of increased ecological value, such as distinguishing leaves from woody material, or parameters relating to the health of vegetation. This work has demonstrated the potential of neural networks for providing a rapid radiometric calibration of raw intensities from a novel TLS sensor to realistic values of apparent reflectance, successfully accounting for the complexities of TLS intensity response. The use of neural networks for this purpose has provided an alternative approach to calibration which can be benchmarked against existing methods in the future.

Although neural networks are essentially 'black boxes' – the user's interaction is limited to defining the inputs, architecture, and outputs – the advantage is that the user does not have to be an expert to use this approach or interpret the results, nor have any prior knowledge about the system.

This research has provided the first description of the radiometric characteristics of a unique dual-wavelength TLS, highlighting the effect of internal temperature on intensity response. This has been shown to be significant for the SALCA instrument, particularly for the middle-infrared wavelength. It may also be important with other TLS, especially for the increasing number of custom-designed and dual/multi-wavelength systems where accurate intensities will be key to quantitative analysis of the data.

Acknowledgements

The authors would like to thank the Forest Commission at Delamere for allowing access to the field site. This study builds on work undertaken with the Terrestrial Laser Scanning International Interest Group (TLSIIG; http://tlsiig.bu.edu/) as part of an instrument inter-comparison experiment held in Brisbane, Australia, in August 2013.

Disclosure statement

No potential conflict of interest was reported by the authors.

Funding

Lucy Schofield was supported by a UK Natural Environment Research Council (NERC) research studentship.

References

Abdi, H., V. Valentin, and B. Edelman. 1999. *Neural Networks*. Thousand Oaks, CA: Sage.

Balduzzi, M., D. Van Der Zande, J. Stuckens, W. Verstraeten, and P. Coppin. 2011. "The Properties of Terrestrial Laser System Intensity for Measuring Leaf Geometries: A Case Study with Conference Pear Trees (*Pyrus Communis*)." *Sensors* 11 (12): 1657–1681. doi:10.3390/s110201657.

Danson, F. M., R. Gaulton, R. Armitage, M. Disney, O. Gunawan, P. Lewis, G. Pearson, and F. Ramirez. 2014. "Developing a Dual-Wavelength Full-Waveform Terrestrial Laser Scanner to Characterize Forest Canopy Structure." *Agricultural and Forest Meteorology* 198–199: 7–14. doi:10.1016/j.agrformet.2014.07.007.

Douglas, E. S., J. Martel, Z. Li, G. Howe, K. Hewawasam, R. A. Marshall, C. L. Schaaf, et al. 2015. "Finding Leaves in the Forest: The Dual-Wavelength Echidna Lidar." *IEEE Geoscience and Remote Sensing Letters* 12 (4): 776–780. doi:10.1109/LGRS.2014.2361812.

Gaulton, R., F. M. Danson, F. Ramirez, and O. Gunawan. 2013. "The Potential of Dual-Wavelength Laser Scanning for Estimating Vegetation Moisture Content." *Remote Sensing of Environment* 132 (0): 32–39. doi:10.1016/j.rse.2013.01.001.

Hakala, T., J. Suomalainen, S. Kaasalainen, and Y. Chen. 2012. "Full Waveform Hyperspectral Lidar for Terrestrial Laser Scanning." *Optics Express* 20 (7): 7119–7127. doi:10.1364/OE.20.007119.

Hancock, S., J. Armston, Z. Li, R. Gaulton, P. Lewis, M. Disney, F. M. Danson, et al. 2015. "Waveform Lidar over Vegetation: An Evaluation of Inversion Methods for Estimating Return Energy." *Remote Sensing of Environment* 164: 208–224. doi:10.1016/j.rse.2015.04.013.

Höfle, B. 2014. "Radiometric Correction of Terrestrial Lidar Point Cloud Data for Individual Maize Plant Detection." *IEEE Geoscience and Remote Sensing Letters* 11 (1): 94–98. doi:10.1109/LGRS.2013.2247022.

Höfle, B., and N. Pfeifer. 2007. "Correction of Laser Scanning Intensity Data: Data and Model-Driven Approaches." *ISPRS Journal of Photogrammetry and Remote Sensing* 62 (6): 415–433. doi:10.1016/j.isprsjprs.2007.05.008.

Kaasalainen, S., A. Jaakkola, M. Kaasalainen, A. Krooks, and A. Kukko. 2011. "Analysis of Incidence Angle and Distance Effects on Terrestrial Laser Scanner Intensity: Search for Correction Methods." *Remote Sensing* 3 (12): 2207–2221. doi:10.3390/rs3102207.

Kaasalainen, S., A. Krooks, A. Kukko, and H. Kaartinen. 2009. "Radiometric Calibration of Terrestrial Laser Scanners with External Reference Targets." *Remote Sensing* 1 (3): 144–158. doi:10.3390/rs1030144.

Kaasalainen, S., A. Kukko, T. Lindroos, P. Litkey, H. Kaartinen, J. Hyyppä, and E. Ahokas. 2008. "Brightness Measurements and Calibration with Airborne and Terrestrial Laser Scanners." *IEEE Transactions on Geoscience and Remote Sensing* 46 (2): 528–534. doi:10.1109/TGRS.2007.911366.

Kaasalainen, S., U. Pyysalo, A. Krooks, A. Vain, A. Kukko, J. Hyyppä, and M. Kaasalainen. 2011. "Absolute Radiometric Calibration of ALS Intensity Data: Effects on Accuracy and Target Classification." *Sensors* 11 (12): 10586–10602. doi:10.3390/s111110586.

Li, Z., A. Strahler, D. Jupp, C. Schaaf, G. Howe, K. Hewawasam, S. Chakrabarti, T. Cook, I. Paynter, and E. Saenz (2015). "Calibration of a Full-Waveform, Dual-Wavelength Terrestrial Laser Scanner." Proceedings of SilviLaser 2015, Le Grande Motte, France, September 28–30 2015.

Pfeifer, N., B. Höfle, C. Briese, M. Rutzinger, and A. Haring. 2008. "Analysis of the Backscattered Energy in Terrestrial Laser Scanning Data." *The International Archives of Photogrammetry, Remote Sensing and Spatial Information Science* 37: 1045–1052.

Ramirez, F., R. Armitage, and F. M. Danson. 2013. "Testing the Application of Terrestrial Laser Scanning to Measure Forest Canopy Gap Fraction." *Remote Sensing* 5 (6): 3037–3056. doi:10.3390/rs5063037.

Wagner, W., J. Hyyppä, A. Ullrich, H. Lehner, C. Briese, and S. Kaasalainen. 2008. "Radiometric Calibration of Full-Waveform Small-Footprint Airborne Laser Scanners." *Presented at The International Archives of the Photogrammetry, Remote Sensing and Spatial Information Sciences, Beijing, China* 2008 (XXXVII): 163–168.

Wagner, W., A. Ullrich, V. Ducic, T. Melzer, and A. Sudnicka. 2006. "Gaussian Decomposition and Calibration of a Novel Small-Footprint Full-Waveform Digitising Airborne Laser Scanner." *Journal of Photogrammetry and Remote Sensing* 60 (2): 100–112. doi:10.1016/j.isprsjprs.2005.12.001.

Welford, D., and A. Mooradian. 1982. "Output Power and Temperature Dependence of the Linewidth of Single-Frequency CW (Gaai) as Diode Lasers." *Applied Physics Letters* 40 (10): 865–867. doi:10.1063/1.92945.